Shape and Extent of the Void Formed by a Horizontal Jet in a Fluidized Bed

Libin Chen and Herbert Weinstein
Dept. of Chemical Engineering, City College of the City University of New York, New York, NY 10031

The introduction of reactant gas into a fluidized-bed chemical reactor as a jet is a common design practice. However, the shape and extent of the void formed by a jet into a fluidized bed and the manner in which the void breaks up into bubbles have still not been described well.

An experimental study of a horizontal jet into a 15 cm by 38 cm cross-section fluidized bed was carried out using an X-ray system. Instantaneous solid fraction averaged along 15-cm chords across the bed were measured. The mean value and the fluctuating component of solid fraction were determined for two initial jet diameters, 0.64 and 1.27 cm, and three initial jet velocities, 23, 46 and 69 m/s. Maps of the mean solid fraction and of statistical properties of the fluctuating component show that there are three discernible regions in the jet-influenced area of the bed. These are a coherent void, bubble trains, and a surrounding compaction zone.

Introduction

In industrial fluidized-bed reactors, reactant gas is often introduced into a reactor as a horizontally directed jet. Understanding the dynamics of the gas and solid motion resulting from the introduction of the jet can have considerable significance for improving reactor design.

The literature to date reveals little of the dynamic behavior of gas and solid arising from a horizontal jet. Lummi and Baskakov (1967) injected a CO_2 tracer with an air jet and measured subsequent CO_2 concentrations in the bed to obtain mixing rates. Zenz (1968) presented a curve to predict horizontal jet penetration depth. Shakhova (1968) derived an expression for horizontal jet penetration depth. Kozin and Baskakov (1967) proposed a penetration correlation which referred to a specific design of a cap-type air distributor. Merry (1971) measured the penetration depths of horizontal air jets injected into fluidized beds of sand, kale seed and steel shot and derived a simple model for jet penetration depth. These workers were mainly concerned with the expression for jet penetration depth. The dynamics of a jet discharged into a fluidized bed was reported on by Shakhova and Minakev (1971), using the ratio of the length of the gas plume to the height of the fluid bed above the nozzle to describe two characteristic modes of jet behavior, bubble flow and coherent flow. Two recent articles by Xuerub et al. (1991a,b) described the behavior of thin, two-dimensional, horizontal and inclined jets. They showed several important jet characteristics such as the proclivity of bubble tracks to hug the wall through which the jet is introduced. Further, they discussed the existence of a dragging zone of particles from the dense phase into the jet near the injection zone. However, the behavior of a two-dimensional system is expected to be quite different from that of a three-dimensional system because, in the latter case, this is a path for gas and solid to move around the sides of the jet. This prevents the jet ceiling from becoming a stagnant zone as it does in the two-dimensional geometry where the jet and the bubble track isolate the ceiling from the rest of the bed. Thus, the extent of the void formed by the three-dimensional horizontal jet and its coherence or integrity, as well as the distortion of the fluidized bed by the jet flow is still not understood well. Furthermore, a general technique for identifying the gas jet flow region and the bubble track region based on measurement is still lacking.

The objective of this work is to investigate the hydrodynamic behavior of a three-dimensional fluidized bed with a horizontal gas jet. The technique employed is to use an X-ray system to obtain maps of the mean and fluctuating solid fraction. With these maps the extent of the void formed by the horizontal jet

Correspondence concerning this article should be addressed to H. Weinstein.

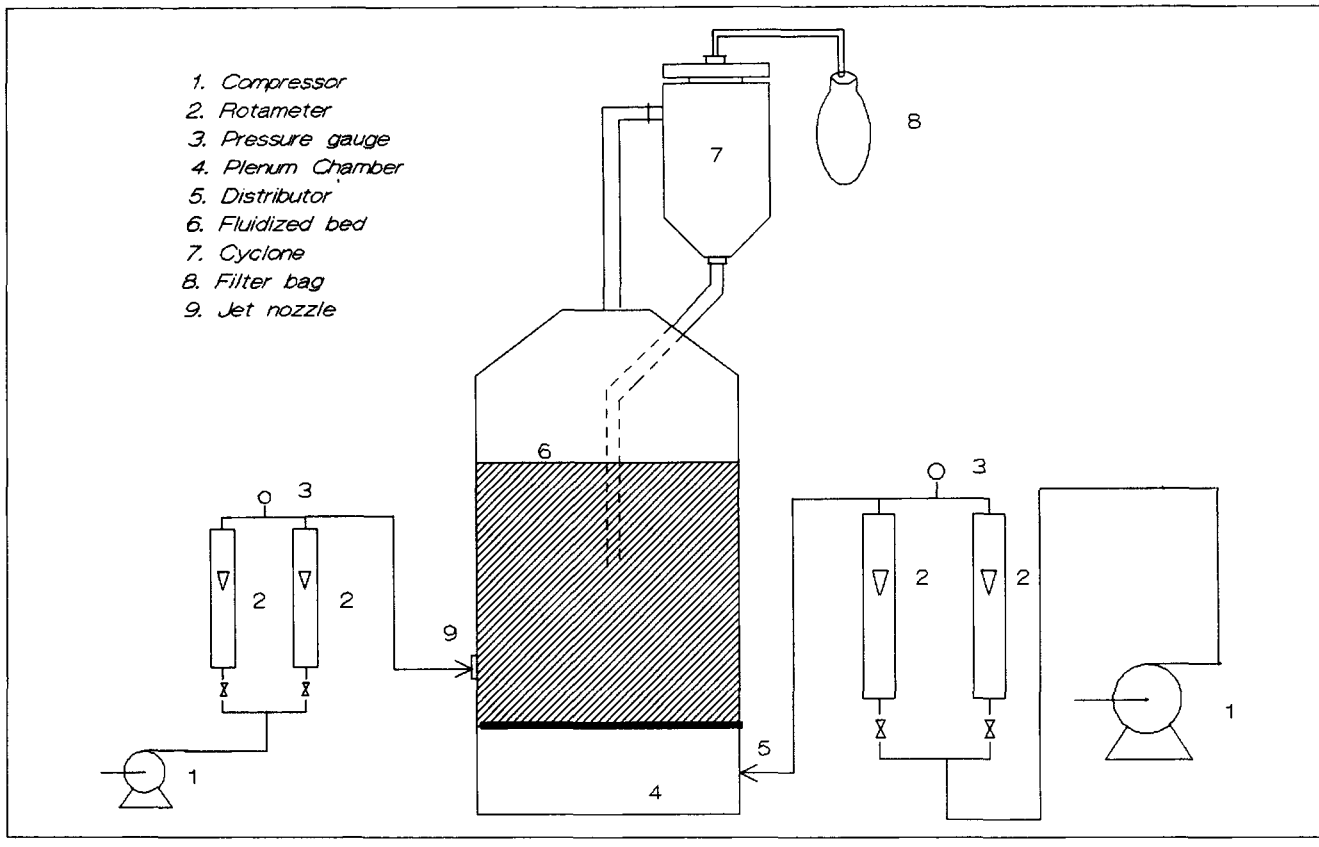

Figure 1. Experimental apparatus.

and the region compacted by the entrained gas can be obtained. Furthermore, the regions of coherent jet flow and bubbling bed flow can be determined from the autocorrelation and power spectrum of the fluctuating signal. Finally, jet penetration correlations from the literature are compared with the unique X-ray data obtained in this work.

Experimental Studies

Apparatus

A schematic diagram of the apparatus used is shown in Figure 1. The bed was contained in a rectangular vessel of Plexiglas, with dimensions 0.15 m × 0.38 m × 1.22 m high. A cyclone was located at the gas outlet of the vessel and exhaust from the cyclone passed through a bag filter. The solid disengaged in the cyclone was returned to the bed through a dipleg. The fluidized height was maintained at about 0.85 m. The solid powder was an Englelhard HFZ-33 FCC cracking catalyst, and its properties are given in Table 1. The fluidizing gas used for the experiment was air at ambient conditions. Rotameters were fitted into the line to meter the air-flow rate. The superficial fluidizing velocity was held at 0.04 m/s for the experiment. A circular jet nozzle module, either 0.64 or 1.27 cm in diameter, was located 0.31 m above the gas distributor. The jet was injected horizontally into the fluidized bed using a second metered compressed air supply.

An X-ray absorption system was used to obtain the solid fraction mean and fluctuation data. The system is described in detail by Feindt (1990). The X-ray source was designed for continuous output and high intensity operation. The X-ray image of the bed was projected onto an 23-cm image intensifier screen. It converted the X-ray into visible light and projected it onto a 8 cm output screen. A mirror with an angle of 45° to the screen projected 90% of the light onto a curved 15 cm screen through a lens. The screen was equipped with 48 phototransistors, all at equal distance from the image intensifier screen. Of these, 13 phototransistors were arranged in a row scanning the projected image of the bed across a horizontal plane were used, as shown in Figure 2. The entire X-ray system was mounted on a platform that could be moved up and down along the vessel.

Data analysis

The measurement principle is based on the Lambert-Beer law:

$$dI = -\mu I ds \tag{1}$$

Table 1. Solid Properties for Engelhard FCC Catalyst, HFZ-33

Mean Particle Size, d_p (μm)	59
Particle Size Range, (μm)	20 ~ 120
Sphericity (ϕ)	1
Particle Density (kg/m^3)	1,450
Minimum Fluidization Velocity u_{mf} (cm/s)	0.9*
Minimum Void Fraction	0.48

*Measured value.

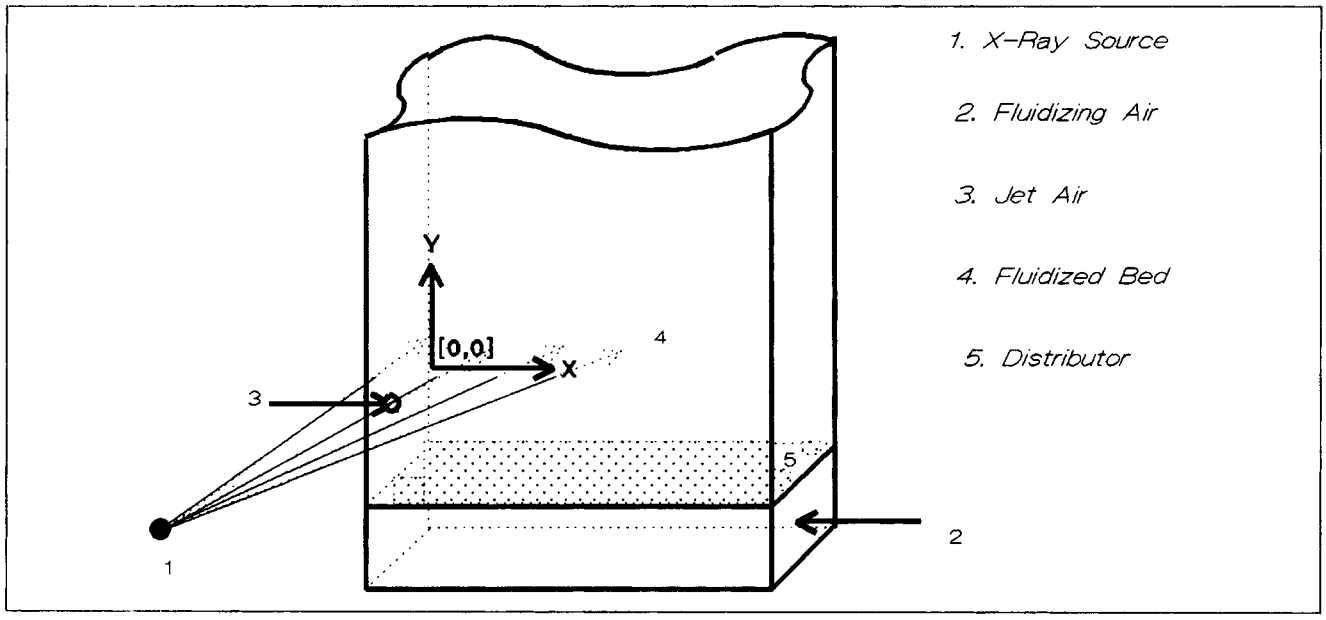

Figure 2. X-ray adsorption system.

where dI is the change of the intensity of the beam passing through the adsorbing medium, s is the length of beam passing through the absorbing medium, and μ is the attenuation coefficient.

Introducing k for the mass attenuation coefficient and ρ for the medium density:

$$\mu = k \cdot \rho \tag{2}$$

In the system, Eq. 1 can be expressed as:

$$\ln \frac{I_{[w+s]}}{I_0} - \ln \frac{I_w}{I_0} = -\int_s k\rho\xi(x, y)ds \tag{3}$$

where s is the chord length and ξ is the local solid fraction.

Therefore, the instantaneous solid fraction at any desired elevation and horizontal position can be obtained by averaging on a chord through the 0.15-m thickness of the bed used, assuming that the attenuation coefficient of the air is negligible.

The voltage-time signals corresponding to the changes of intensity were sampled at the rate of 50 Hz by a Dell 386/20 mHz computer with an Metra-byte Das-20 analog-to-digital converter board. By means of Eq. 3, the signals were converted to instantaneous solid fraction signals. The data acquired in this way was used to calculate the mean values, the autocorrelation functions, the power spectrum and the normalized standard deviations of the solid fraction values.

The mean solid fraction through the bed was computed as:

$$1 - \bar{\epsilon} = \frac{1}{T}\int_0^T (1-\epsilon)dt \tag{4}$$

The difference between the time-mean solid fraction of the bubbling bed without the jet and with the jet was interpreted as a void or "hole" resulting from the jet gas in the bed:

$$\bar{\epsilon}_J - \bar{\epsilon}_B = (1-\bar{\epsilon})_B - (1-\bar{\epsilon})_J \tag{5}$$

This term is called herein the solid fraction decrement. In order to use this data to calculate the statistical properties of the solid fraction, we define a fluctuating component (ϵ') as:

$$1 - \epsilon = (1-\bar{\epsilon}) - (1-\epsilon)' \tag{6}$$

and

$$-(1-\epsilon)' = \epsilon' \tag{7}$$

since a fluctuation in solid fraction is the negative of a fluctuation in void fraction.

The standard deviation (rms) of the apparent solid fraction fluctuation, σ, normalized by the X-ray mean value of the solid fraction (NSD) can be expressed as:

$$\text{NSD} = \frac{\sigma}{1-\bar{\epsilon}} \tag{8}$$

The autocorrelation function and the autocorrelation coefficient can also be expressed, respectively, as:

$$R_{\epsilon'}(\tau) = \lim_{T\to\infty} \frac{1}{T}\int_0^T \epsilon'(t)\epsilon'(t+\tau)dt \tag{9}$$

$$\rho_{\epsilon'}(\tau) = \frac{R_{\epsilon'}(\tau)}{\sigma^2} \tag{10}$$

The power spectral density function can also be calculated by the fast Fourier transform (FFT):

$$S_{\epsilon'}(f) = \int_{-\infty}^{\infty} R_{\epsilon'}(\tau)e^{-j2\pi f\tau}d\tau \tag{11}$$

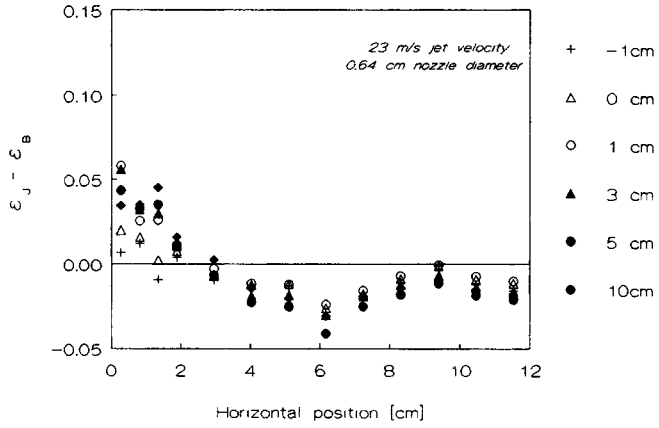

Figure 3a. Solid fraction decrement as a function of horizontal position with vertical position as parameter: 23-m/s jet velocity; 0.64-cm nozzle diameter.

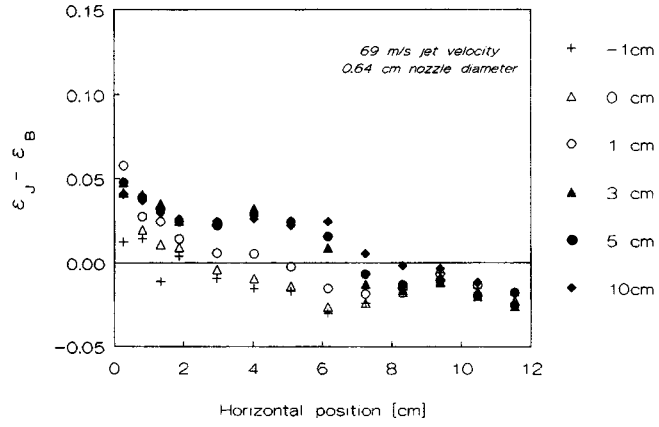

Figure 3b. Solid fraction decrement as a function of horizontal position with vertical position as parameter: 69-m/s jet velocity; 0.64-cm nozzle diameter.

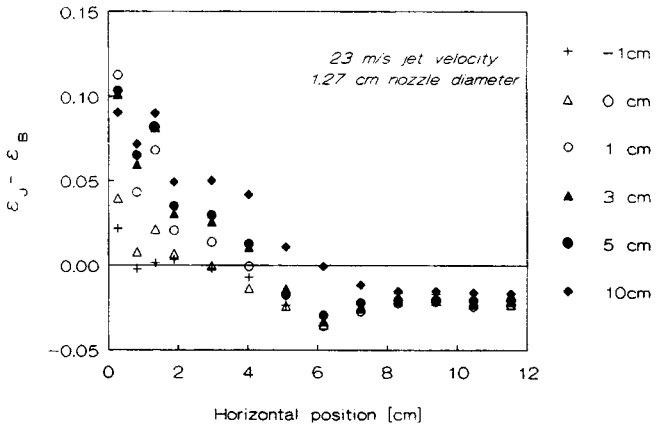

Figure 3c. Solid fraction decrement as a function of horizontal position with vertical position as parameter: 23-m/s jet velocity; 1.27-cm nozzle diameter.

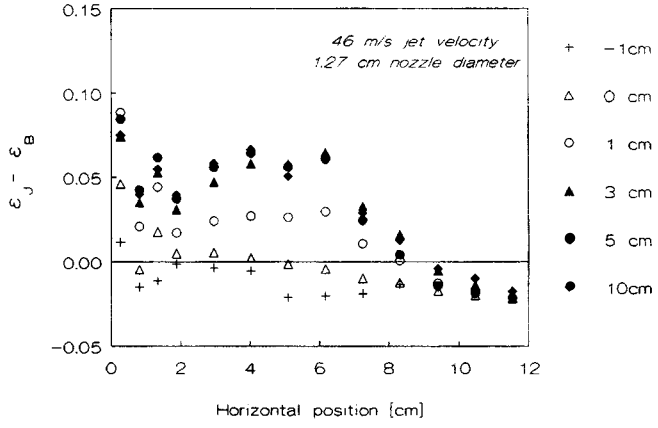

Figure 3d. Solid fraction decrement as a function of horizontal position with vertical position as parameter: 46-m/s jet velocity; 1.27-cm nozzle diameter.

and then, multiplying the complex spectrum by its complex conjugate, $S^*_{\epsilon'}$, yielding:

$$\text{PSDF} = \overline{S_{\epsilon'} \cdot S^*_{\epsilon'}} = \overline{S^2_{\epsilon'}} \tag{12}$$

For each run, the instantaneous solid fraction with the jet turned on and with the jet turned off at 78 different vertical and horizontal positions were obtained by moving the X-ray imaging system up and down along the bed. At each selected location, a set of 9,216 data points were obtained for every experimental run. This set corresponds to about a 3-min record length, which was found experimentally to be sufficient to give a true steady-state value.

Results and Discussion

Four experimental series were carried out with the two jet nozzles, comprising two different jet velocities for each jet diameter: for the 0.64-cm nozzle, 23 and 69 m/s; for the 1.27-cm nozzle, 23 and 46 m/s.

Extent of the void formed by the horizontal jet

Mean solid fraction decrements as a function of horizontal position with vertical position as a parameter are plotted in Figures 3a–3d. These figures indicate the locations at which the void fractions are increased and decreased by the presence of the jet. The origin, (0, 0), corresponds to the center of the nozzle position. As seen from these maps, the horizontal jet void discharges one or more bubble trains from its upper surface. The bubble trains do not all leave from the far end of the void. One chain of bubbles is stabilized along the nozzle wall of the vessel. In addition, other bubble trains emerge from the void over its length. It is also seen from these figures that the length of the void or hole increases with increasing jet momentum, and the bubble trains move further from the nozzle. Furthermore, the solid fraction decrements in the void region increase with the increasing mass-flow rate of the gas jet. This indicates that the dimension of the hole parallel to the X-ray beam path also increases.

Two other observations of some importance can be made from these figures. The first is that the jet void curves upward

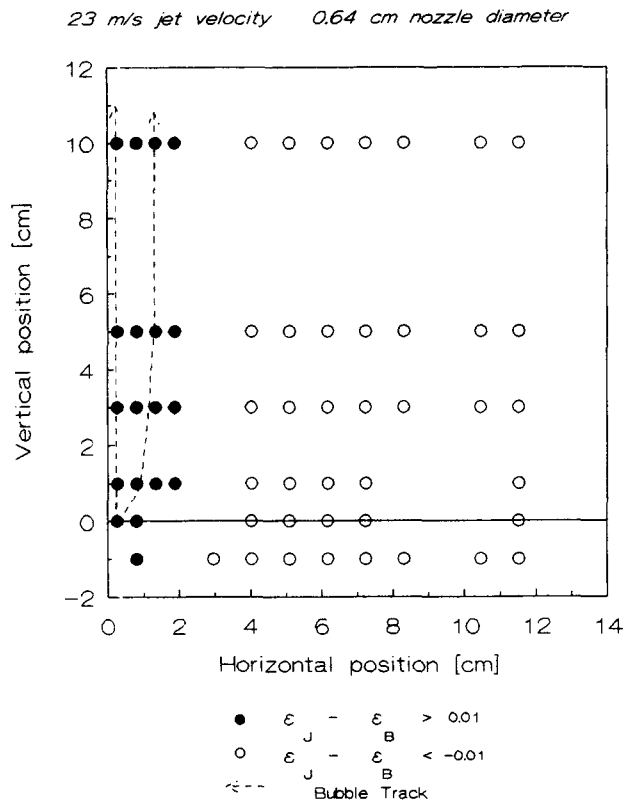

Figure 4a. Void, bubble track, and compaction regions: 23-m/s jet velocity; 0.64-cm nozzle diameter.

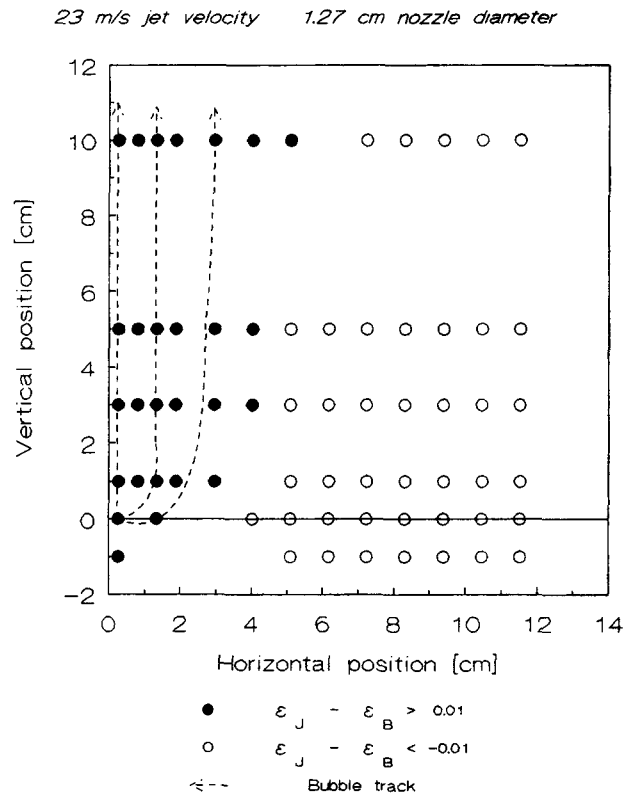

Figure 4c. Void, bubble track, and compaction regions: 23-m/s jet velocity; 1.27-cm nozzle diameter.

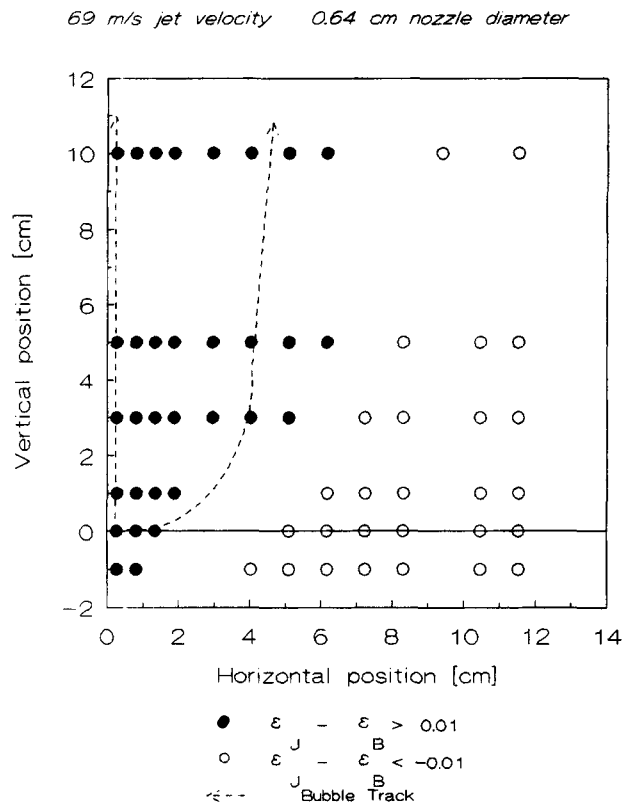

Figure 4b. Void, bubble track, and compaction regions: 69-m/s jet velocity; 0.64-cm nozzle diameter.

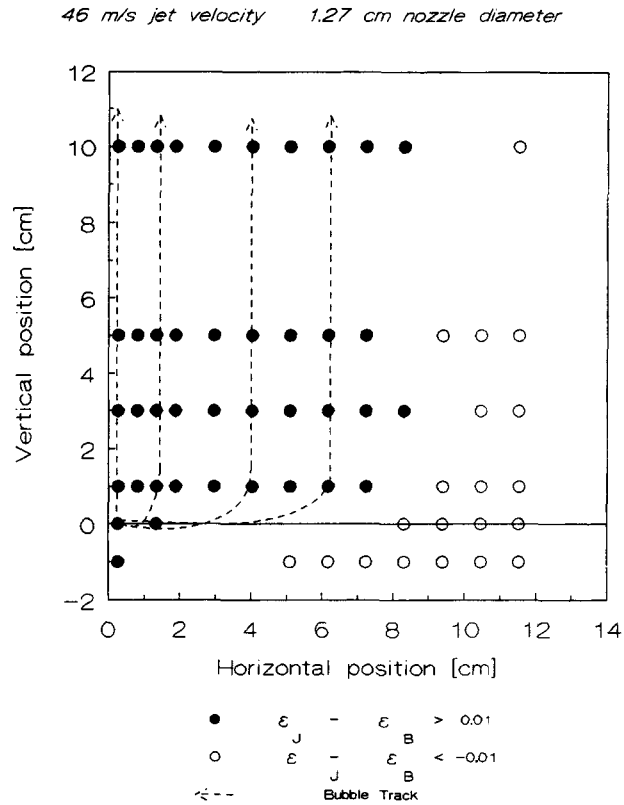

Figure 4d. Void, bubble track, and compaction regions: 46-m/s jet velocity; 1.27-cm nozzle diameter.

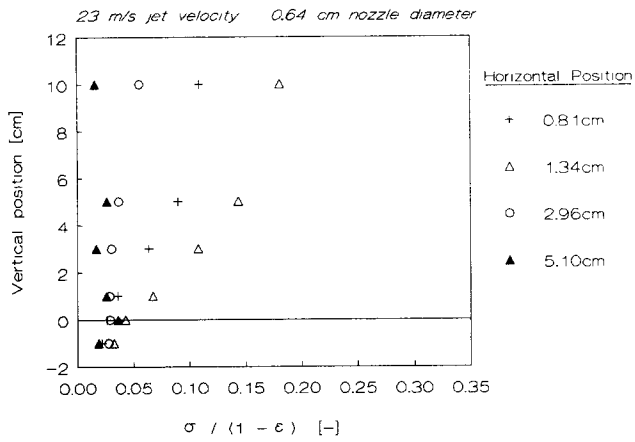

Figure 5a. Normalized standard deviation of solid fractions horizontal position as parameter: 23-m/s jet velocity; 0.64-cm nozzle diameter.

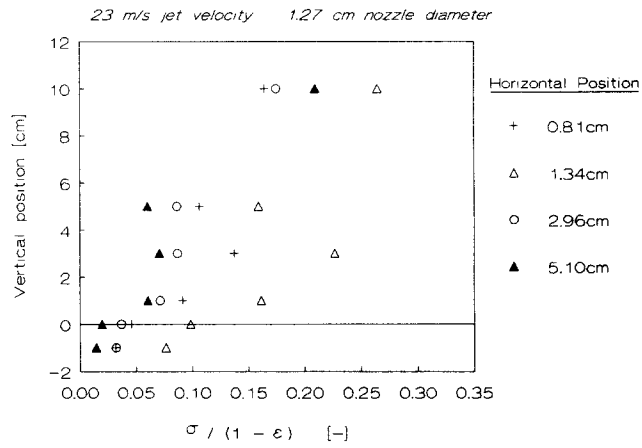

Figure 5c. Normalized standard deviation of solid fractions horizontal position as parameter: 23-m/s jet velocity; 1.27-cm nozzle diameter.

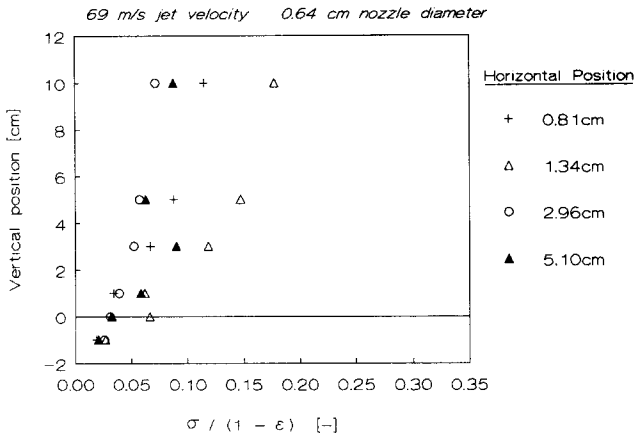

Figure 5b. Normalized standard deviation of solid fractions horizontal position as parameter: 69-m/s jet velocity; 0.64-cm nozzle diameter.

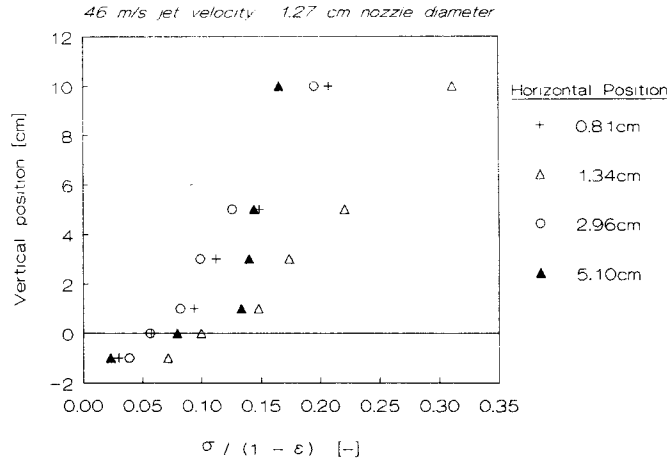

Figure 5d. Normalized standard deviation of solid fractions horizontal position as parameter: 46-m/s jet velocity; 1.27-cm nozzle diameter.

away from the nozzle, as would be expected. The second is that the jet entrains gas from the bed underneath and to the right of the jet void causing a wake-like compaction (negative solid fraction decrement) of the solid. This latter point will be discussed in a later section.

The data shown in Figure 3 are replotted in Figures 4a–4d by marking horizontal and vertical position with solid circles where the solid fraction decrements are larger than 0.01. Also plotted as open circles are the locations at which the decrement is negative. The dashed lines represent the bubble track paths. Examination of these figures leads to the conclusion that jet gas entering the bed produces a void region along the top of which bubble trains are discharged. In the case of the lower jet velocity, for the nozzle diameter of 0.64 cm two trains of bubbles are formed. Both of them are located close to the vessel wall. In the case of the higher velocity, one of the two bubble trains moves farther away, about 4 cm from the wall, as indicated by an arrow in Figure 4b, widening the high voidage area. For the nozzle diameter of 1.27 cm, both jet velocities have higher mass-flow rates than the two cases with the 0.64-m nozzle diameter, establishing more bubble paths with higher voidage, as shown in Figure 4c and Figure 4d. In these figures, it is also seen that one train of bubbles still stayed close to the end wall, while the others moved farther out along the jet axis.

A statistical analysis of the solid fraction fluctuation signals yields further confirmation of these results. The normalized standard deviations of the fluctuation as a function of vertical position with horizontal position are plotted in Figures 5a–5d, respectively. In Figure 5a, the smallest air flow rate in the experimental range, the solid fraction fluctuation signals recorded at both 2.96 and 5.1 cm away from the wall did not change along the bed height. This means that the jet did not discharge bubbles to these regions. However, the signals at the position near the wall showed large fluctuations, especially at 1.34 cm away from the wall. As mentioned above, this was the path of bubble train. In Figure 5d, the largest flow rate in the experimental range, signals received from every position all showed extremely large fluctuations which indicated that bubble trains passed through all measured positions and covered a large region. The picture of the bubble region discharged

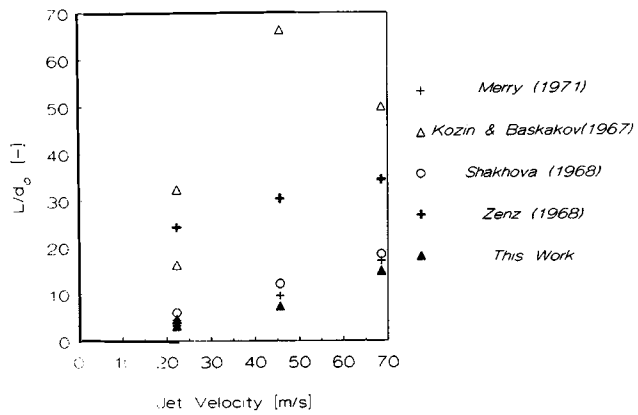

Figure 6. Comparison of experimental data for jet penetration length with predicted values.

from the jet derived from Figures 5a–5d is similar to that derived from Figures 4a–4d. Thus, there is agreement between the bubble track paths obtained from the mean void fraction with those obtained from the standard deviation of the fluctuation.

Penetration length

To define a jet penetration length, it was assumed that the jet did not penetrate beyond the horizontal position at which all solid fraction decrements were measured at different vertical positions within ± 0.015. This value was chosen empirically, because it appeared to always separate the void-bubble train zone on the right from the compaction zone. Using this definition of penetration length, the experimental penetration length was compared with the values predicted by various correlations as plotted in Figure 6. The figure shows that the experimental data agreed well with the data predicted by the correlations of Merry (1971), as well as Shakhova (1968). The experimental data also confirmed Merry's conclusions that the penetration depth increases with nozzle diameter and jet nozzle velocity. The data of Xuereb et al. (1991a) also agreed reasonably well with the correlations of Merry and Shakhova.

Compacted region formed by the horizontal jet

Another characteristic region of the jet field, the compacted solid or wake region, is also illustrated by the figures discussed above. From Figures 3a–3d or Figures 4a–4d, it can be seen that the compacted region, which is shown by negative solid fraction decrements is extensive. This region forms because the pressure in the lower part of the void formed by the jet is lower than that in the surrounding two-phase region. The gas from the bed is entrained into the void and bubble trains. This compacted bed region below the void appears to be similar in nature to the wake below a bubble in a fluidized bed. Furthermore, as the bubble trains rise, the upper part solid carried up by the bubbles moves back down to the right of the train compacting this region of the bed. The compaction appears to be particularly strong in the regions below and just beyond jet void penetration. It appears that this compacted region coincides with the dragging zone of particles described by Xuereb et al. (1991a).

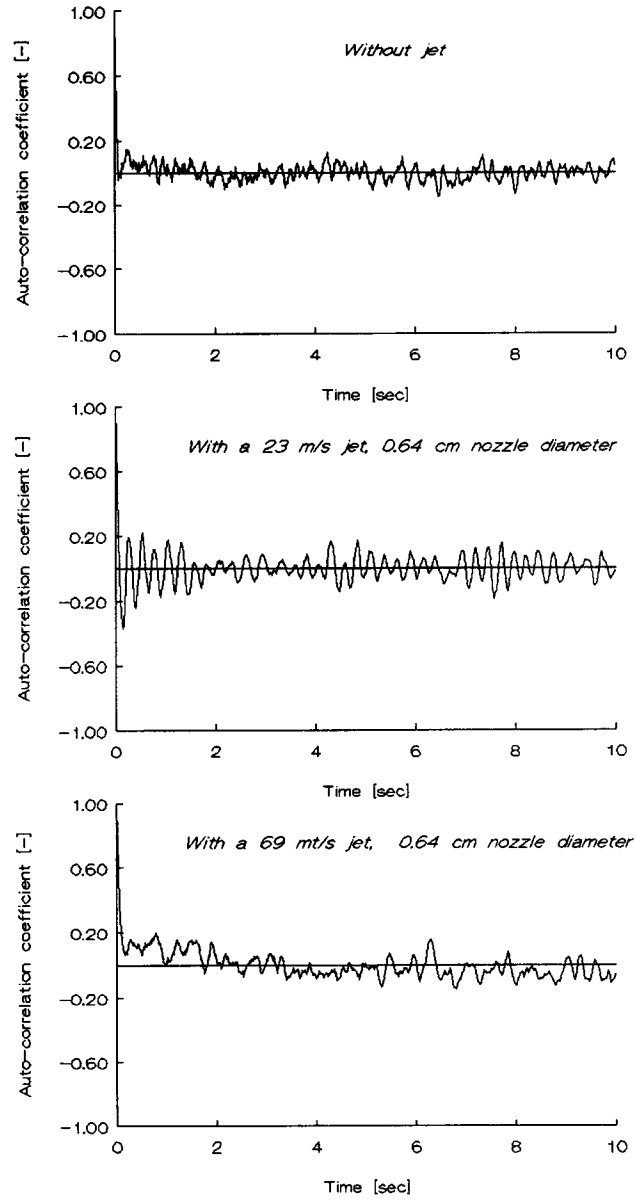

Figure 7. Comparison of autocorrelation function at a fixed position: $Y = 1$ cm, $X = 1.34$ cm.

Differentiation between void, bubbles and compaction regions

The presence of a periodic component in the solid fraction fluctuations at a location in the bed is indicative of the presence of a bubble train. Thus, by comparing the auto-correlation functions of signals at the different positions, the locations of jet void and bubble train can be differentiated. The upper graphs in Figures 7 and 8 show the signals from the fluidized bed without a jet, while the middle and lower graphs show signals with different velocity jets. Figure 7 shows that a periodic oscillation of the signal is present at (1 cm, 1.34 cm) with the 23-m/s jet, but this is not present without the jet or with the 69 m/s jet. Similar to Figure 7, Figure 8 shows periodicity only with the 69 m/s at (3 cm, 5.1 cm). As can be seen in Figure 3a, the 23-m/s jet has a strong solid fraction decrement at the point (1 cm, 1.34 cm). Coupling the two

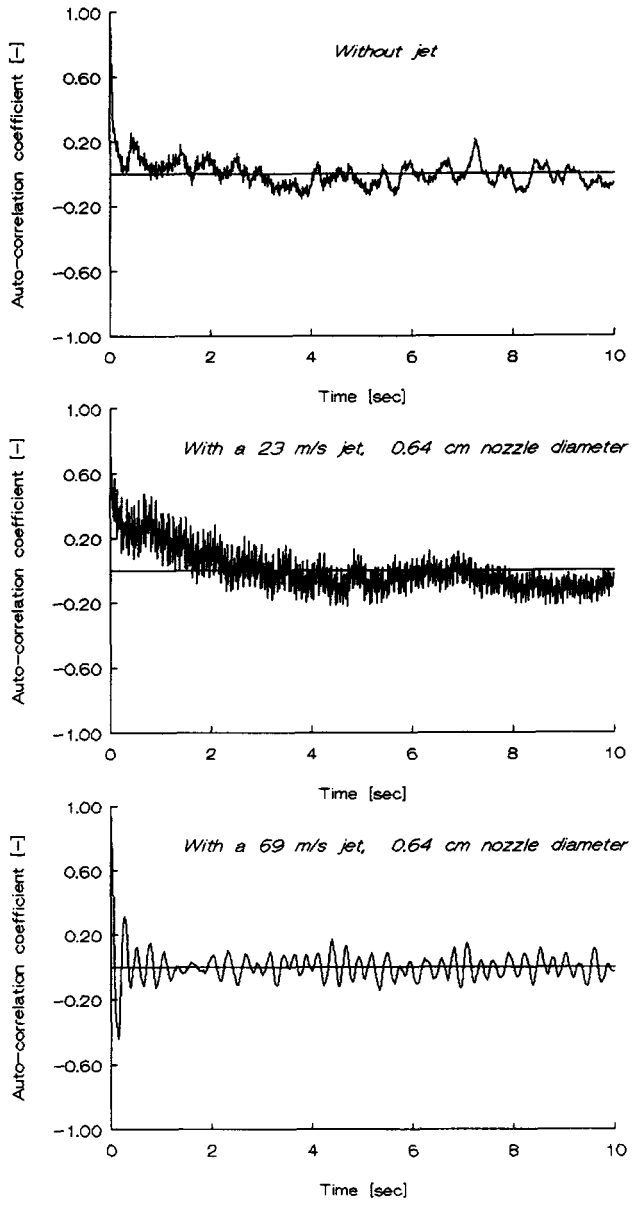

Figure 8. Comparison of autocorrelation function at a fixed position: $Y = 3$ cm; $X = 5.1$ cm.

pieces of information supports the conclusion that a bubble train has already formed at this point. For the 69-m/s case, the solid fraction decrement is also large but the apparent lack of periodicity, as shown by the autocorrelation, leads to the conclusion that the coherent void occupies this space. Further away from the nozzle, the point at (3 cm, 5.1 cm), Figure 8 shows an autocorrelation function consistent with the compaction zone shown in Figure 3a for the 23-m/s jet. However, for the high velocity jet, the autocorrelation function shows a bubble train consistent with the large solid fraction decrement shown at this point in Figure 3b.

Another characteristic feature for identifying a coherent void, bubble track or compacted region is the power spectrum of the fluctuations of solid fraction. Figure 9 shows the power spectrum calculated from the same signals as that of Figure 8. There is a single major frequency peak in the power spectrum

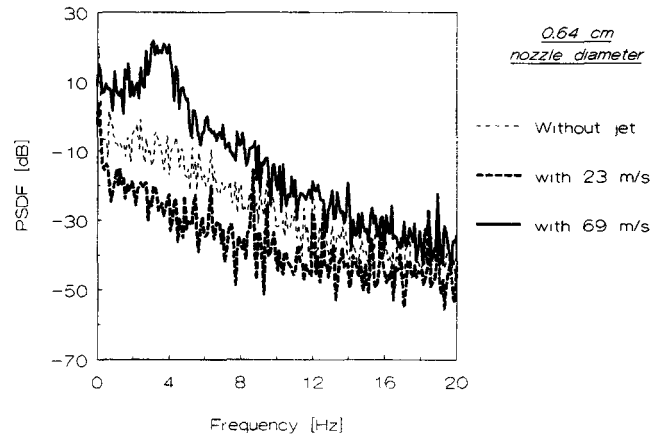

Figure 9. Comparison of power spectral density function of solid fraction fluctuation signals at a fixed position: $Y = 3$ cm; $X = 5.1$ cm.

with the 69-m/s jet, which represents the characteristic frequency of the periodic component of the fluctuations in the bubble track. Due to the random component in the compacted region, such as solid entrained by the jet, no clear frequency peak is observed in the power spectrum of the signals with the 23-m/s jet. The power spectrum for a coherent void, which is not shown, also does not exhibit any characteristic peak region. This analysis is in agreement with the results of the autocorrelation functions. Consequently, for identification of the various regions in the fluidized bed formed by the horizontal jet, this method is proposed which utilizes the distinctive features of the mean solid fraction decrement, the autocorrelation functions and the power spectrum functions of fluctuating signals.

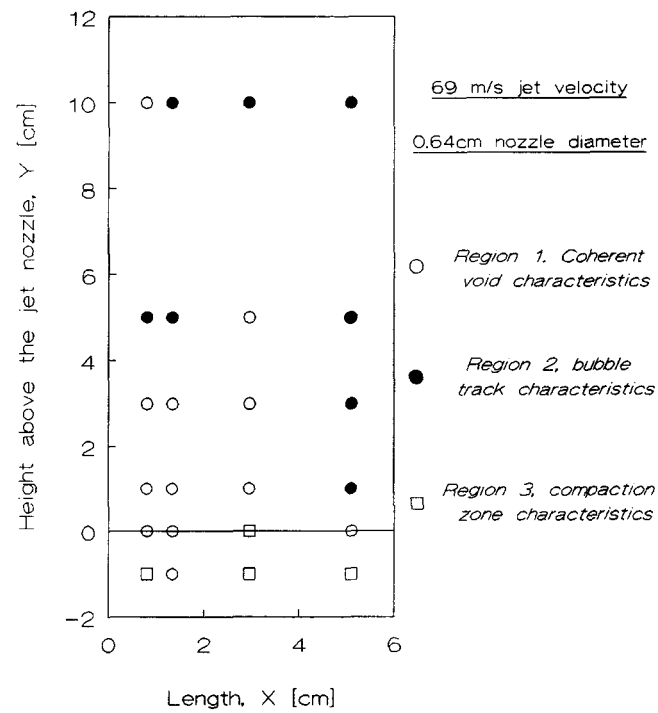

Figure 10. Map of flow regions: 69-m/s jet velocity; 0.64-cm nozzle diameter.

Based on this methodology, a description of the individual regions can be constructed. A typical flow region map obtained by analyzing the autocorrelation functions is shown in Figure 10. As schematically displayed in this figure, three regions can be located in the X-ray field. Region 1 is the coherent void region, which does not show the periodicity typical of bubble trains. The bubble track region is region 2. The jet gas leaves the coherent void region as bubbles and the autocorrelation functions in the tracks show a clear periodic shape. The compacted region, 3, results from the wakelike behavior under and to the right of the void and the downflow of solids to the right of the bubble tracks. As shown in Figure 8, the autocorrelation function in this region also does not exhibit a clear periodic pattern.

Conclusions

The following conclusions can be drawn from the analysis of the experimental results presented herein:

- This experimental technique clearly shows that the horizontal jet forms three regions in the fluidized bed: a coherent void, bubble trains, and a surrounding compaction zone.
- Wake jets turn upward close the inlet wall and form bubble trains along the wall. Strong jets penetrate deeper into the bed and form multiple bubble trains which leave from across the upper surface of the void.
- The jet penetration lengths measured agreed with the correlations of Merry (1971) and Shakhova (1968).

Notation

d_0 = nozzle diameter, m
d_p = mean particle diameter, m
dI = change of the intensity of the beam passing through the adsorbing medium
g = acceleration of gravity, m/s^2
I = intensity of X-ray beam
I_0 = intensity of the reference X-ray beam
I_s = intensity of X-ray beam passing through the solid
I_w = intensity of X-ray beam passing through the wall of the bed
k = mass attenuation coefficient
L = penetration length, m
NSD = normalized standard deviation
PSDF = power spectral density function
$R_{\epsilon'}$ = autocorrelation function
s = chord length
$S_{\epsilon'}$ = Fourier transform of the autocorrelation of ϵ'
u = superficial gas fluidizing velocity, m/s
u_J = jet velocity, m/s
u_{mf} = minimum fluidization velocity, m/s
x = length of beam passing through absorbing medium
X = coordinate, horizontal direction
Y = coordinate, vertical direction

Greek letters

ϵ = void fraction
ϵ_b = void fraction without the jet
ϵ_J = void fraction with the jet
ϵ_{mf} = void fraction at minimum fluidization
μ = attenuation coefficient
ξ = local solid fraction
ρ = density of solid particle, kg/m^3
$\rho_{\epsilon'}$ = autocorrelation coefficient
σ = standard deviation
ϕ = sphericity of the solid particle

Acknowledgment

This work was supported by The Exxon Research and Engineering Company, Florham Park, NJ.

Literature Cited

Feindt, H. J., "Radial and Axial Density Fluctuations in A High Velocity Fluidized Bed," PhD Thesis, City Univ. of New York (1990).
Kozin, B. E., and A. P. Baskakov, *Khim. Tekhnol. Topl. Masel*, **3**, 4 (1967).
Lummi, A. P., and A. P. Baskakov, *Khim. Prom.*, **43**, 7,522 (1967).
Merry, J. M. D., "Penetration of A Horizontal Gas Jet into A Fluidized Bed," *Trans. Instn. Chem. Engrs.*, **49**, 189 (1971).
Shakhova, N. A., *Inzh. Fiz. Zh.*, **14**(1), 61 (1968).
Shakhova, N. A., and G. A. Minayev, "Aerodynamics of Jets Discharged into Fluidized Beds," *Heat Transfer-Sov. Res.*, **4**(1), 133 (1972).
Xuereb, C., C. Laguerie, and T. Baron, "Etude du Comportement de Jets Continus Horizontaux ou Inclines Introduits dans un Lit Fluidise pan un Gaz, Deuxieme Partie: Profils de Vitesse du Vitesse du Gaz dans les Jets Horizontaux," *Powder Technol.*, **64**, 271 (1991).
Xuereb, C., C. Laguerie, and T. Baron, "Etude du Comportement de Jets Continus Horizontaux ou Inclines Introduits dans un Lit Fluidise pan un Gaz, I: Morphologie des Jets," *Powder Technol.*, **67**, 43 (1991).
Zenz, F. A., *Inst. Chem. Eng. Symp.*, ser. 30, p. 136 (1968).

Manuscript received Jan. 22, 1993, and revision received Apr. 19, 1993.